International Communications in Heat and Mass Transfer 110 (2020) 104409

Contents lists available at ScienceDirect

International Communications in Heat and Mass Transfer

journal homepage: www.elsevier.com/locate/ichmt

MHD thermogravitational convection and thermal radiation of a micropolar nanoliquid in a porous chamber

Mohsen Izadi[a], Mikhail A. Sheremet[b,*], S.A.M. Mehryan[c], I. Pop[d], Hakan F. Öztop[e,f], Nidal Abu-Hamdeh[f]

[a] Mechanical Engineering Department, Faculty of Engineering, Lorestan University, Khorramabad, Iran
[b] Laboratory on Convective Heat and Mass Transfer, Tomsk State University, 634050 Tomsk, Russia
[c] Young Researchers and Elite Club, Yasooj Branch, Islamic Azad University, Yasooj, Iran
[d] Department of Mathematics, Babeş-Bolyai University, 400084 Cluj-Napoca, Romania
[e] Department of Mechanical Engineering, Technology Faculty, Firat University, Elazig, Turkey
[f] Department of Mechanical Engineering, King Abdulaziz University, Jeddah, Saudi Arabia

ARTICLE INFO

Keywords:
Natural convection
Magnetic field
Micropolar nanoliquid
Porous cavity
Elliptic heater
Local thermal equilibrium model

ABSTRACT

This work studies the thermogravitational transmission and thermal radiation of micropolar nanoliquid within a porous chamber in the presence of the uniform magnetic influence. The model includes the single-phase nanofluid approach, local thermal equilibrium approximation and Darcy law for the processes within the porous structure. The Galerkin finite element method with the structured non-uniform mesh is used to calculate the formulated equations. The key characteristics are the Darcy–Rayleigh number Ra = 10–1000, Darcy number Da = 10^{-5}–10^{-1}, porosity ε = 0.1–0.9, nanoparticles concentration φ = 0–0.04, radiation parameter R_d = 0–2, vortex viscosity characteristic Δ = 0–2, and Hartmann number Ha = 0–50. It has been ascertained the energy transport intensification with thermal radiation parameter, Darcy–Rayleigh number, porosity and nanoparticles concentration. Also, the results indicate that the average Nusselt number reduces with an increment of the Hartmann number for high values of the Rayleigh number, while for low magnitudes of the Rayleigh number a weak change of the average Nusselt number can be found.

1. Introduction

The convective heat transfer of micropolar fluids is an important topic due to many various applications in description of the flow of slurries, liquid crystals, blood, some polymeric fluids and composite materials [1,2]. The theory of micropolar fluid has been described in detail by Eringen

[3–5]. Nowadays, many different fundamental investigations have been performed for study of convective motion and energy transport in micropolar liquids [6–8]. Thus, Javed and Siddiqui [6] have studied numerically mixed convective circulation and thermal transmission in a chamber with moving border filled with micropolar fluid in the presence of bottom heating and uniform horizontal magnetic influence. It has been found that Hartmann and Reynolds numbers reduce the strength of circulation and isolines of microrotations. Ahmed and Nadeem [7] have investigated numerically MHD micropolar blood circulation in a vertical artery with six various types of stenosis. They have found that the resistance impedance is maximum for the bell-shaped stenosis and minimum for the trapezoidal one. Sheremet et al. [8] have studied unsteady thermogravitational energy transport of micropolar liquid in an irregular triangular chamber by the finite difference method and non-primitive variables. They have shown the thermal transmission intensity diminution and micropolar liquid circulation suppression with the vortex viscosity parameter. Muthtamilselvan et al. [9] have examined numerically thermogravitational convection of micropolar liquid in a cavity with hot thin sheet. The presence of vortex viscosity characteristic suppresses the liquid velocity and hence the thermal transmission intensity. In another paper Muthtamilselvan et al. [10] have conducted a numerical study of double-diffusive thermogravitational energy transport of micropolar liquid in a chamber with a heated thin sheet under the Soret and Dufour effects. They have shown the thermal and solute transport enhancement with characteristics of Soret and Dufour. Natural convective boundary-layer circulation combined with thermal radiation of a micropolar liquid close to a vertical plate in the presence of periodic magnetic impact has been analyzed by Siddiqa et al. [11]. Employing the similarity technique, the control

* Corresponding author.
E-mail address: Michael-sher@yandex.ru (M.A. Sheremet).

https://doi.org/10.1016/j.icheatmasstransfer.2019.104409

Available online 25 November 2019

Nomenclature

B	magnetic field ($kg{\cdot}s^{-2}{\cdot}A^{-1}$)
C_p	specific heat ($J{\cdot}kg^{-1}{\cdot}K^{-1}$)
g	gravitational acceleration ($m{\cdot}s^{-2}$)
H	cavity size (m)
Ha	Hartmann number (−)
I	intensity of a current (A)
j	the micro-inertia density (m^2)
K	permeability of porous medium (m^2)
k	thermal conductivity ($W{\cdot}m^{-1}{\cdot}K^{-1}$)
$\boldsymbol{N}$	non-dimensional microrotation vector (−)
N^*	dimensional microrotation vector (s^{-1})
p	non-dimensional pressure (−)
P^*	dimensional pressure (Pa)
Pr	Prandtl number (−)
Ra	thermal Rayleigh number (−)
T	non-dimensional temperature (−)
T^*	dimensional temperature (K)
u, v	non-dimensional components of velocity in x and y directions, respectively (−)
u^*, v^*	dimensional components of velocity in x^* and y^* directions, respectively ($m{\cdot}s^{-1}$)
$\boldsymbol{V}$	non-dimensional velocity vector (−)
V^*	dimensional velocity vector ($m{\cdot}s^{-1}$)
x, y	non-dimensional Cartesian coordinates (−)
x^*, y^*	dimensional Cartesian coordinates (m)

Greek symbols

α	thermal diffusivity ($m^2{\cdot}s^{-1}$)
β	thermal expansion coefficient (K^{-1})
Δ	vortex to molecular viscosity ratio (−)
ε	porosity (−)
κ	vortex viscosity ($kg{\cdot}m^{-1}{\cdot}s^{-1}$)
μ	dynamic viscosity ($kg{\cdot}m^{-1}{\cdot}s^{-1}$)
ν	kinematic viscosity ($m^2{\cdot}s^{-1}$)
ρ	density ($kg{\cdot}m^{-3}$)
σ	electrical conductivity ($A^2{\cdot}s^3{\cdot}kg^{-1}{\cdot}m^{-3}$)
ϕ	volume fraction of nanoparticles (−)
ψ	non-dimensional stream function (−)
ψ^*	dimensional stream function ($m^2{\cdot}s^{-1}$)

Subscripts

bf	base fluid
c	cold
m	refer to porous structure
nf	nanofluid
np	nanoparticles
s	solid matrix

Supperscripts

*	dimensional variables

equations formulated in the form of ordinary differential equations have been calculated by the Keller-box scheme. The skin friction parameter reduces essentially by rising the micro-inertia density and magnetic interaction characteristics, while the opposite nature can be found when the micropolar parameter and thermal radiation parameter are amplified.

Nowadays, solution of different engineering problems demands the heat transfer enhancement. Such heat transfer intensification can be obtained not only by using the additional heat transfer surfaces but also using the nanofluids. In 1995, the term “nanofluid” has been introduced by Choi [12] to describe dilute suspensions formed by nanoparticles less than 100 nm in diameter created early by Masuda et al. [13]. Therefore, a lot of fundamental works deals with an analysis of energy transport in nanoliquids systems [14–46]. Some papers deal with micropolar nanofluids to demonstrate the microrotation and local behavior of the nanofluid units [47,48]. Thus, Hussanan et al. [49] have studied analytically the time-dependent natural convective circulation of five various kinds of oxide nano-sized particles in a micropolar nanoliquid over a vertical plate. They have shown the effects of different nanoparticles material on the heat transfer enhancement. Taking into account the two-phase nanofluid model proposed by Buongiorno [50], Hayat et al. [51] have described the Brownian circulation and thermophoresis effects on micropolar nanoliquid motion. Stretching sheet with linear velocity defines the nanofluid motion under the influence of the radiation and Newtonian heating. It has been shown that the energy and mass transport intensities are amplified for high magnitudes of the radiation and Brownian diffusion characteristics. In addition, heat transfer through porous media has been the subject of many researches [52–62]. Hashemi et al. [63] have investigated computationally thermogravitational thermal transmission in a copper-water micropolar nanofluid porous chamber in the presence of the internal heat generation. It has been pictured that a raise of the Darcy parameter reflects a weak decrease in the intensity of micropolar nanofluid circulation and micro-rotation of particles, while an increment of the vortex viscosity characteristic results in a diminution of the power of particles microrotation. Conjugate thermogravitational convection of micropolar nanoliquid in a porous chamber on the basis of the local thermal non-equilibrium approach has been examined computationally by Mehryan et al. [47]. It has been ascertained that Nu depends on the vortex viscosity for high Ra and it does not depend on this parameter for low Ra. Bourantas and Loukopoulos [48] have analyzed theoretically the free convective energy transport of micropolar nanofluids inside a square enclosure. Using the experimental data for thermophysical properties the authors have discovered some discrepancies between Nu in the case of different experimental correlations. Mixed convective circulation in a water-based micropolar nanoliquid cavity with moving border under the effect of local heater with constant heat flux has been studied numerically by Ahmed et al. [64]. It has been revealed that Nu at the heater reduces as the heater size rises while it enhances when the nanoparticles concentration augments.

Taking into account the previously studied publications and to the authors' best knowledge, there have been no researches of free convective circulation and energy transport of micropolar nanofluid in a porous enclosure with an internal elliptical heat source. Therefore, the main objective of the present investigation is a numerical study of thermogravitational energy transport of micropolar nanoliquid inside a porous chamber having centrally located heated elliptical cylinder under the impact of uniform magnetic influence and thermal radiation.

2. Mathematical description of the problem

A porous square chamber of H size including an elliptic heater located in the center of the cavity is illustrated in Fig. 1. The domain of interest contains the CuO-H_2O micropolar nanoliquid. A magnetic field determined by B vector with amplitude B_0 and inclination angle γ is affected on the cavity. The third coordinate of the cavity that is perpendicular to the cavity and it is much longer compared with the others. The horizontal boundaries of the cavity are adiabatic, while vertical borders are isothermal with constant temperature $T_c{}^*$. The isothermal elliptical heat source has high constant temperature $T_h{}^*$. Darcy law is considered to define the macroscopic circulation within the chamber. The changes of the chemico-physical parameters of the

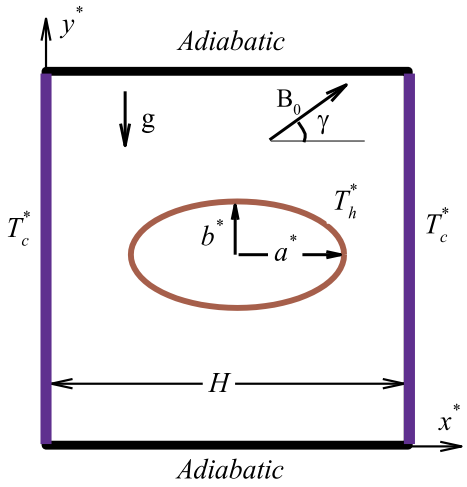

Fig. 1. Domain of interest.

Table 1
The values of coefficients in Eq. (18-d) for CuO-H_2O nanoliquid [73].

The magnitudes of coefficients	CuO-H_2O nanofluid
a_1	−26.5933108
a_2	−0.403818333
a_3	−33.3516805
a_4	−1.915825591
a_5	0.06421858
a_6	48.40336955
a_7	−9.787756683
a_8	190.245610009
a_9	10.9285386565
a_{10}	−0.72009983664

Table 2
Mesh sensitivity analysis.

Elements number	3780	5134	6880	9874	11,440
Nu_{avg}	15.458	15.462	15.461	15.459	15.458
$\|\psi\|_{max}$	3.987	3.985	3.983	3.982	3.982

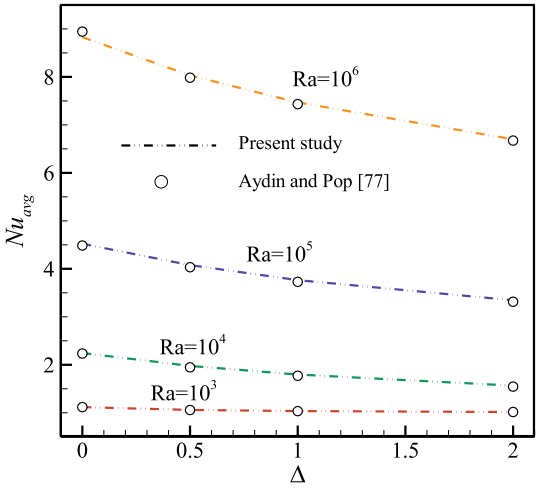

Fig. 2. The average Nusselt number in comparison with numerical results of Aydin and Pop [77].

base liquid and solid particles material are supposed to be negligible expect for the density, where the Boussinesq approximation is valid. Local thermal equilibrium approach is assumed between the liquid and solid structures of the system. The solid particles and base liquid are considered to be equilibrated in the case of velocity and temperature fields. The micro-rotations for micropolar liquid are modeled by including the angular momentum vector to the Navier-Stokes equations considering the volumetric forces appearing due to rotations at micro-level [6,8,47]. Additionally, for the description of the thermal radiation effect the Rosseland approximation is used [65].

Taking into account these models, the control equations are formulated in the following form [66,67]:

$$\nabla\cdot\boldsymbol{V}^* = 0 \tag{1}$$

$$0 = -\nabla^* p^* - \frac{\mu_{nf} + \kappa}{K}\boldsymbol{V}^* - (\rho\beta)_{nf}(T^* - T_c^*)\mathbf{g} + \kappa\nabla^*\times\boldsymbol{N}^* + \boldsymbol{I}\times\boldsymbol{B} \tag{2}$$

$$\nabla^*\cdot\boldsymbol{I} = 0 \tag{3}$$

$$\boldsymbol{I} = \sigma_{nf}(-\nabla^*\Phi + \boldsymbol{V}^*\times\boldsymbol{B}) \tag{4}$$

$$\rho_{nf} j(\boldsymbol{V}^*\cdot\nabla^*)\boldsymbol{N}^* = \left(\mu_{nf} + \frac{\kappa}{2}\right) j\nabla^{*2}\boldsymbol{N}^* + \frac{\kappa}{\varepsilon}\nabla^*\times\boldsymbol{V}^* - 2\kappa\boldsymbol{N}^* \tag{5}$$

$$(\rho C_p)_{nf}(\boldsymbol{V}^*\cdot\nabla^* T^*) = k_{m,nf}\nabla^{*2} T^* - \nabla^*\cdot\boldsymbol{q_r} \tag{6}$$

where q_r is

$$\boldsymbol{q_r} = -\frac{4}{3}\frac{\sigma_e}{\beta_R}\nabla^* T^{*4} \text{ and } T^{*4} = 4T_c^{*3}T^* - 3T_c^{*4} \tag{7}$$

In these equations the bold letters are the vector parameters. Also, j is the micro-inertia density and $j = L^2$, $k_{m,nf}$ is the effective thermal conductivity of the porous structure [68]:

$$k_{m,nf} = (1-\varepsilon)k_s + \varepsilon k_{nf} \tag{8}$$

where k_{nf} and k_s are the thermal conductivity of the micropolar nanoliquid and solid matrix of the porous system, respectively, and ε is the porosity.

Combining Eqs. (3) and (4) taking into account Garandet et al. [69] we have

$$\nabla^{*2}\Phi = 0 \tag{9}$$

Supposing that cavity borders are electrically insulated, Eq. (9) has the following solution

$$\nabla^*\Phi = 0 \tag{10}$$

Excluding the pressure gradient in motion Eq. (2) and introducing new dependent variable, stream function ($u_{nf}^* = \partial\psi^*/\partial y^*, v_{nf}^* = -\partial\psi^*/\partial x^*$), two motion equations can be written as expressed below:

$$\frac{\mu_{nf}+\kappa}{K}\left(\frac{\partial^2\psi^*}{\partial x^{*2}} + \frac{\partial^2\psi^*}{\partial y^{*2}}\right) = g(\rho\beta)_{nf}\frac{\partial T^*}{\partial x^*} + \kappa\left(\frac{\partial^2 N^*}{\partial x^{*2}} + \frac{\partial^2 N^*}{\partial y^{*2}}\right) - \sigma_{nf}B_0^2\left(\frac{\partial^2\psi^*}{\partial y^{*2}}\sin^2\gamma + 2\frac{\partial^2\psi^*}{\partial x^*\partial y^*}\sin\gamma\cos\gamma + \frac{\partial^2\psi^*}{\partial x^{*2}}\cos^2\gamma\right) \tag{11}$$

For non-dimensionalization, the following non-dimensional variables are employed:

$$x = x^*/H,\quad y = y^*/H,\quad \psi = \psi^*/\alpha_{m,bf},\quad T_{nf} = (T_{nf}^* - T_c^*)/(T_h^* - T_c^*),\quad N = (L^2/\alpha_{m,bf})N^* \tag{12}$$

Therefore, one can find

$$\frac{\partial^2\psi}{\partial x^2} + \frac{\partial^2\psi}{\partial y^2} = -Ra\frac{(\rho\beta)_{nf}}{(\rho\beta)_{bf}}\left(\frac{1}{\mu_r+\Delta}\right)\frac{\partial T}{\partial x} + Da\left(\frac{\Delta}{\mu_r+\Delta}\right)\left(\frac{\partial^2 N}{\partial x^2} + \frac{\partial^2 N}{\partial y^2}\right) - Ha^2\left(\frac{\sigma_r}{\mu_r+\Delta}\right)\left(\frac{\partial^2\psi}{\partial y^2}\sin^2\gamma + 2\frac{\partial^2\psi}{\partial x\partial y}\sin\gamma\cos\gamma + \frac{\partial^2\psi}{\partial x^2}\cos^2\gamma\right) \tag{13}$$

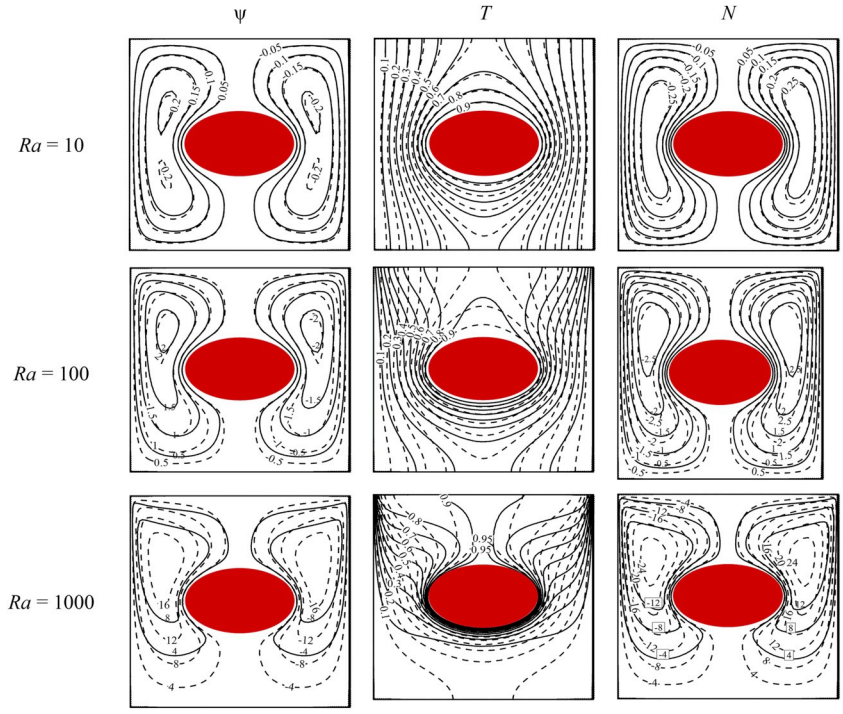

Fig. 3. Streamlines ψ, isotherms T and isolines of microrotation N for different values of the Rayleigh number at $R_d = 0$ (solid lines) and $R_d = 2$ (dashed lines), $\phi = 0.02$, $\varepsilon = 0.5$, $Da = 10^{-2}$, $\Delta = 1$, $Ha = 0$.

Table 3
Average *Nu* magnitudes for porous triangular cavity filled with Cu-H_2O nanoliquid.

Ra	ϕ	Sun and Pop [76]	Sheremet et al. [8]	Present work
500	0	9.66	9.65	9.64
1000	0.1	9.42	9.41	9.42
500	0	13.9	14.05	13.96
1000	0.2	12.85	12.84	12.85

$$\frac{\partial\psi}{\partial y}\frac{\partial N}{\partial x}-\frac{\partial\psi}{\partial x}\frac{\partial N}{\partial y}=Pr\left(\frac{\rho_{bf}}{\rho_{nf}}\right)\left(\mu_r+\frac{\Delta}{2}\right)\left(\frac{\partial^2 N}{\partial x^2}+\frac{\partial^2 N}{\partial y^2}\right)-2\,Pr\,\Delta\left(\frac{\rho_{bf}}{\rho_{nf}}\right)N+\frac{\Delta\,Pr}{\varepsilon}\left(\frac{\rho_{bf}}{\rho_{nf}}\right)\left(\frac{\partial^2\psi}{\partial x^2}+\frac{\partial^2\psi}{\partial y^2}\right) \tag{14}$$

$$\frac{\partial\psi}{\partial y}\frac{\partial T}{\partial x}-\frac{\partial\psi}{\partial x}\frac{\partial T}{\partial y}=\left(\frac{\alpha_{m,nf}}{\alpha_{m,bf}}+\frac{4}{3}\frac{(\rho C_p)_{bf}}{(\rho C_p)_{nf}}R_d\right)\left(\frac{\partial^2 T}{\partial x^2}+\frac{\partial^2 T}{\partial y^2}\right) \tag{15}$$

Here Ra, Da, Pr, Ha, μ_r, σ_r, Δ, R_d, and $\alpha_{m,nf}$ are

$$Ra=\frac{g\beta_{bf}(T_h^*-T_c^*)KH}{\alpha_{bf}\nu_{bf}},\quad Da=\frac{K}{H^2},\quad \mathrm{Pr}=\frac{\nu_{bf}}{\alpha_{bf}},\quad Ha=B_0\sqrt{\frac{\sigma_{bf}K}{\mu_{bf}}},$$
$$\mu_r=\frac{\mu_{nf}}{\mu_{bf}},\quad \sigma_r=\frac{\sigma_{nf}}{\sigma_{bf}},\quad \Delta=\frac{\kappa}{\mu_{bf}},\quad R_d=\frac{4\sigma_e T_e^3}{\beta_R k_{m,bf}},\quad \alpha_{m,nf}=\frac{k_{m,nf}}{(\rho C_p)_{nf}} \tag{16}$$

The boundary conditions are:

$$\begin{aligned}&\psi=0,\quad N=0,\quad T=0 \quad \text{on the left and right vertical walls}\\ &\psi=0,\quad N=0,\quad \frac{\partial T}{\partial y}=0 \quad \text{on the upper and bottom walls}\\ &\psi=C,\quad N=0,\quad T=1 \quad \text{on the elliptic heater}\end{aligned} \tag{17}$$

Koo-Kleinstreuer-Li (KKL) approach [70,71] is used to define the nanoliquid chemico-physical parameters:

$$k_{nf}=k_{Static}+k_{Brownian} \tag{18-a}$$

$$\frac{k_{Static}}{k_{bf}}=1+\frac{3\left(\frac{k_{np}}{k_{bf}}-1\right)\phi}{\left(\frac{k_{np}}{k_{bf}}+2\right)-\left(\frac{k_{np}}{k_{bf}}-1\right)\phi} \tag{18-b}$$

$$\frac{k_{Brownian}}{k_{bf}}=5\times10^4\phi(\rho C_p)_{bf}\left(\frac{\kappa_b T}{\rho_{bf}d_{np}}\right)^{0.5}g'(\phi,T,d_p) \tag{18-c}$$

$$\begin{aligned}&g'(\phi,T,d_{np})\\&=(a_1+a_2\ln(d_{np})+a_3\ln(\phi)+a_4\ln(d_{np})\ln(\phi)+a_5\ln(d_{np})^2)\ln(T)\\&+(a_6+a_7\ln(d_{np})+a_8\ln(\phi)+a_9\ln(d_{np})\ln(\phi)+a_{10}\ln(d_{np})^2)\end{aligned} \tag{18-d}$$

$$R_f+\frac{d_{np}}{k_{np}}=\frac{d_{np}}{k_{np,eff}},\ R_f=4\times10^{-8}\ m^2{\cdot}K/W \tag{18-e}$$

$$\mu_{nf}=\frac{\mu_{bf}}{(1-\phi)^{2.5}}+\frac{k_{Brownian}}{k_{bf}}\frac{\mu_{bf}}{Pr} \tag{19}$$

The other thermophysical parameters of the nanoliquid are [72]:

$$\begin{aligned}&\rho_{nf}=(1-\phi)\rho_{bf}+\phi\rho_{np},\quad \alpha_{nf}=\frac{k_{nf}}{(\rho C_p)_{nf}},\\&(\rho\beta)_{nf}=(1-\phi)(\rho\beta)_{bf}+\phi(\rho\beta)_{np},\\&(\rho C_p)_{nf}=\phi(\rho C_p)_{np}+(1-\phi)(\rho C_p)_{bf}\end{aligned} \tag{20}$$

Parameters for the additional function g' presented in Eq. (18-d) for the CuO-water nanofluid can be seen in Table 1.

3. Procedure of solution, grid independency test and validation

A numerical technique based on the Galerkin finite element is used for computations. Detailed discussion of the employed computational algorithm is in [74,75]. Initially the grid independence test has been performed for the following parameters $Ra = 10^3$, $\varepsilon = 0.5$, $Da = 10^{-2}$,

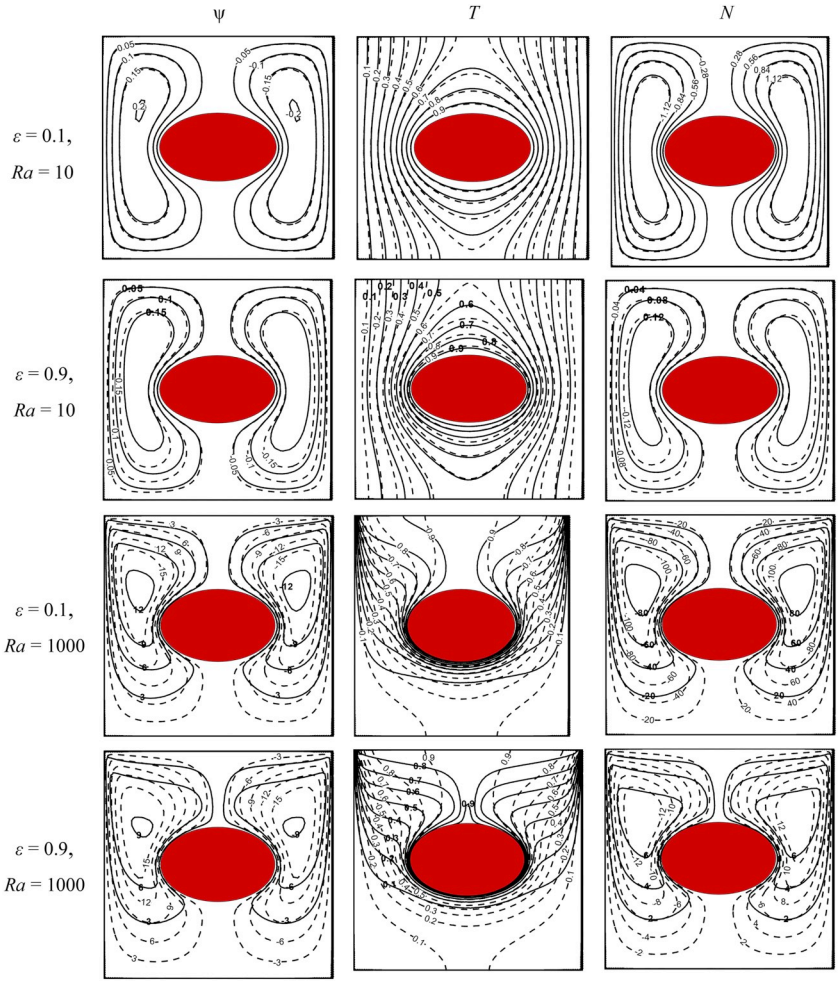

Fig. 4. Streamlines ψ, isotherms T and isolines of microrotation N for various Rayleigh numbers and porosities at $R_d = 0$ (solid lines) and $R_d = 2$ (dashed lines), $\phi = 0.02$, $Da = 10^{-2}$, $\Delta = 1$, $Ha = 0$.

$\Delta = 1$, $R_d = 1$, $Ha = 10$, $\gamma = \pi/2$ and $\phi = 0.04$. The data of this validation, as presented in Table 2, characterize that a mesh of 9874 elements is enough for analysis.

In the case of benchmark analysis several problems from literature [47,76,77] have been studied using the developed numerical technique. A good agreement has been obtained that can be found in Figs. 2, 3 and Table 3.

4. Results and discussion

Analysis of the control characteristics influence (Darcy–Rayleigh number $Ra = 10$–1000, porosity $\varepsilon = 0.1$–0.9, Darcy number $Da = 10^{-5}$–10^{-1}, radiation parameter $R_d = 0$–2, nanoparticles concentration $\phi = 0$–0.04, vortex viscosity characteristic $\Delta = 0$–2, Hartmann number $Ha = 0$–50) on the velocity and temperature fields as well as the rates of thermal transmission has been performed.

Fig. 3 shows the impact of radiation characteristic on isolines of stream function, temperature, and micro-rotations at various Ra. The effect of radiation parameter on these characteristics increases with increasing in Ra. A raise of the Rayleigh number breaks the symmetry between the flow and the horizontal centerline passing through the cavity owing to the domination of convective energy transport over the conductive heat transfer. In general, the flow rate rises for high Ra, considering the radiation parameter. The radiative and molecular diffusions change the patterns of isothermal lines and temperature distribution (see Eq. (15)). On the other hand, the radiative diffusion can reduce the flow viscosity and resistance against fluid movement, thereby increasing the flow rate. These conditions can result in a greater flow mixture throughout the enclosure and improve the cooling and heat transfer parameters. Finally, the angular momentum affecting the liquid volumes inside the pores of the porous system increases with a raise of the radiation characteristic and flow rate at high Rayleigh numbers, increasing the micro-rotation power.

Fig. 4 demonstrates the influence of radiation number on streamlines, isothermal lines, and isomicrorotations at different porosities. According to this figure, the influence of this characteristic on the streamlines and micro-rotations increases with increasing in the porosity at low Rayleigh numbers. It seems that a greater volume of fluid is affected by the radiative heat transfer at an increased porosity coefficient. In addition, the resistance against the nanofluid particle movement reduces with reducing the viscosity, resulting in a weak increment of the circulation intensity. Moreover, the angular momentum affecting the liquid volumes increases with a growth of the porosity coefficient under the radiation effects, thereby increasing the micro-rotation power. In contrast, the effect of radiation parameter can be seen at both high and low porosity with increasing in the Rayleigh number and buoyancy forces. According to the first and second rows, an increase in the porosity does not significantly affect the streamlines at low Rayleigh numbers. In contrast, an increase in the porosity (the third and fourth rows) reduces the power of flow lines at high Ra. In addition, the reduction in micro-rotation power is intensified with increasing the porosity. This reduction is owing to a reduction of the angular momentum affecting the liquid volumes with increasing in the size of porous medium's pores. The effect of an increase in the porosity on the

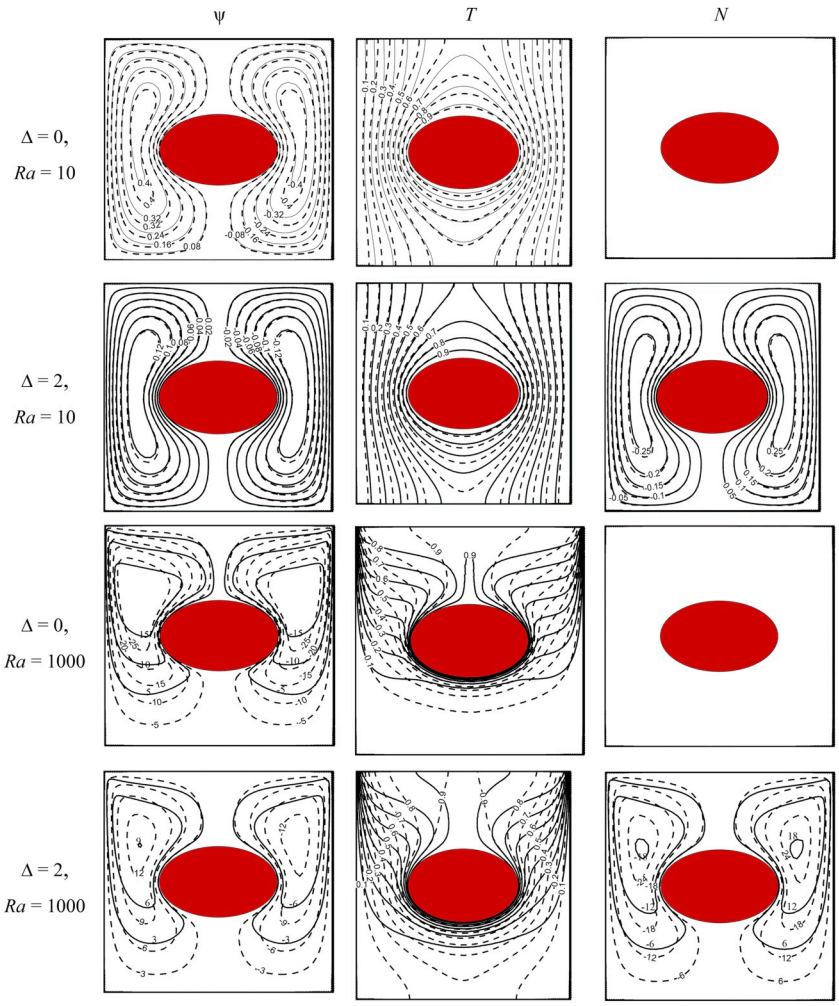

Fig. 5. Streamlines ψ, isotherms T and isolines of microrotation N for various Rayleigh numbers and vortex viscosity at $R_d = 0$ (solid lines) and $R_d = 2$ (dashed lines), $\phi = 0.02$, $\varepsilon = 0.5$, $Da = 10^{-2}$, $Ha = 0$.

isothermal lines is reflected as a reduction in the boundary layer thickness, specifically in the region above the elliptical heater, where the greater concentration of the isothermal lines can increase the Nusselt number with increasing the porosity.

Fig. 5 shows the impacts of radiation number and vortex viscosity on isolines of stream function, isotherms and isolines of micro-rotations at different Rayleigh numbers. Application of vortex viscosity, along with molecular viscosity, increases the resistance against fluid particle movement and reduces the flow rate. These conditions apply to both high and low Rayleigh numbers. However, a greater reduction in the flow rate is observed at lower Rayleigh numbers.

This is because the effect of resistance to particle movement is greater at lower buoyancy force. In addition, the influence of radiation characteristic on the isotherms significantly rises with increasing in *Ra*, resulting in a significant change in temperature distribution.

Fig. 6 demonstrates the impact of *Ha* and *Ra* on isolines of stream function, temperature, and micro-rotations. According to this figure, a growth of *Ha* at both high and low Rayleigh numbers not only reduces the flow rate, but also results in an overall change in the flow pattern. The Lorentz force acts in an opposite direction to the buoyancy forces, reducing the power of streamlines. The effect of radiation parameter is reduced with the application of magnetic field, specifically at high Rayleigh numbers, and the streamlines overlap for different radiation parameters. Also, it can be observed a similar micro-rotation behavior. The angular momentum affecting the liquid volumes, caused by the buoyancy force, reduces with the application of the angular momentum in an opposite direction, caused by the Lorentz force, resulting in reduced micro-rotation power. The isotherms distortion, caused by an increase in the buoyancy force, significantly rises with increasing in the Rayleigh number from 10 to 10^3 and results in a longitudinal stretch, indicating a growth of the natural convective heat transfer. However, the effect of radiation parameter on the isotherms significantly reduces with increasing in the Lorentz force resistance to the fluid particle movement and decreasing in the flow rate at $Ra = 10^3$ and $Ha = 50$.

Fig. 7 illustrates *Nu* changes with the radiation parameter and Rayleigh number. According to this figure, the Nusselt number rises with a growth of *Ra* and radiation parameter. An amplification of *Ra* increases the circulation intensity and natural convective energy transport. An increase in the radiation parameter (Fig. 3) changes the isothermal lines, resulting in a rise of *Nu*.

Fig. 8 shows the mean *Nu* changes with R_d and ϕ at various *Ra*. According to this figure, although *Nu* is relatively independent on ϕ at a low *Ra* ($Ra = 10$), it increases with a growth of ϕ at high Rayleigh number ($Ra = 10^3$). The effect of nanoparticles inclusion to the host liquid amplifies with a growth of the Rayleigh number. In fact, a rise of nano-sized particles concentration results in a slight increase in the thermal diffusion of nanofluid and therefore, increases mean Nusselt number.

Fig. 9 presents the changes of the mean *Nu* with radiation parameter and porosity at two different Rayleigh numbers. According to this figure, Nu_{avg} raises with increasing in the porosity. The shear stress acting on the nanofluid particles in the cavity reduces with increasing

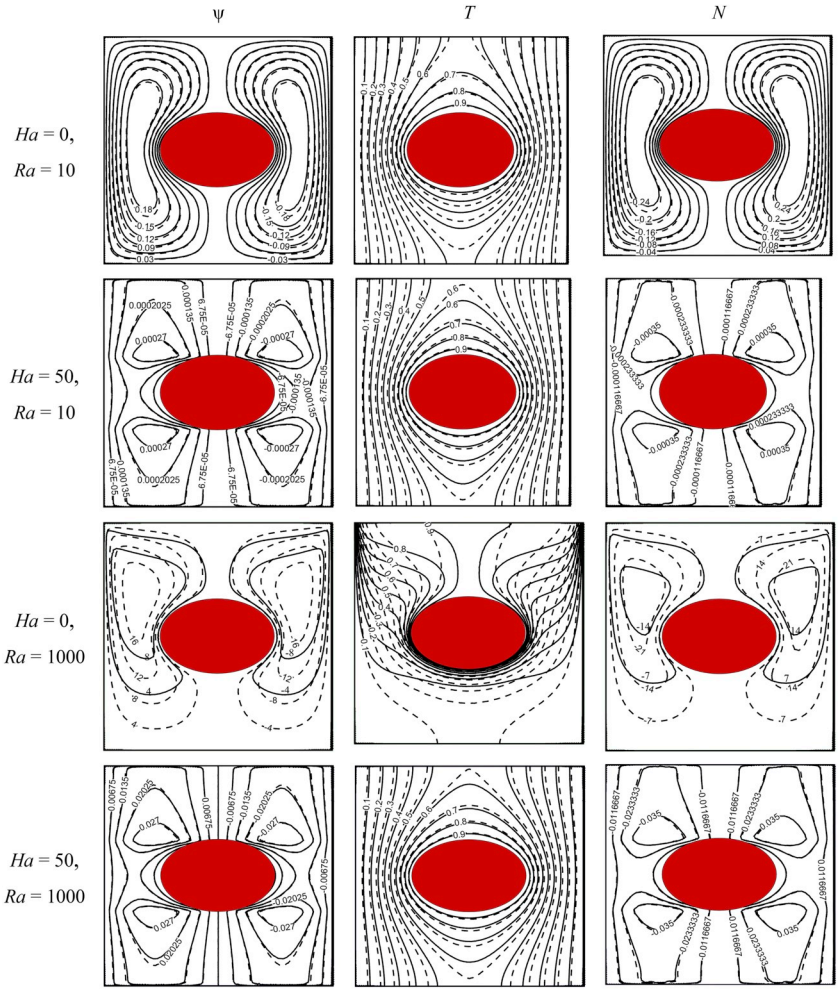

Fig. 6. Streamlines ψ, isotherms T and isolines of microrotation N for various Rayleigh and Hartmann numbers at $R_d = 0$ (solid lines) and $R_d = 2$ (dashed lines) at $\phi = 0.02$, $\varepsilon = 0.5$, $Da = 10^{-2}$, $\Delta = 1$.

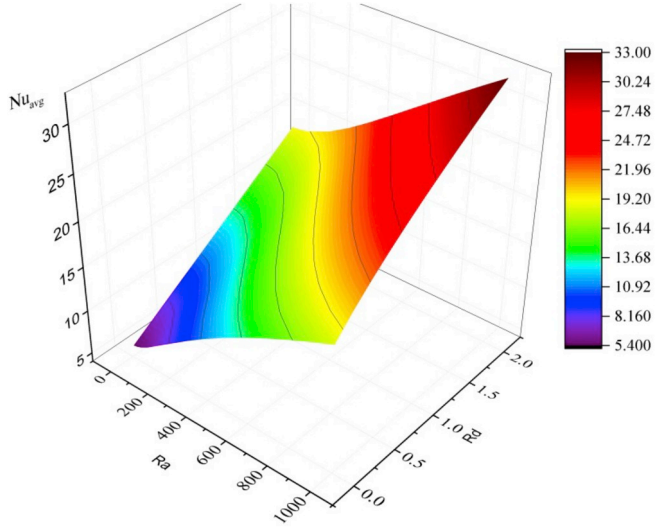

Fig. 7. Changes of Nu_{avg} with radiation characteristic and Rayleigh number.

the porosity and size of the porous medium's pores, reducing the resistance against fluid particle movement. This phenomenon increases the flow power and improves the convective heat transfer.

Fig. 10 indicates the independence of the mean Nusselt number from vortex viscosity at low Ra ($Ra = 10$). In contrast, the mean Nu reduces with increasing in the vortex viscosity at higher Rayleigh number ($Ra = 10^3$). This behavior suggests that the influence of vortex viscosity on the convective thermal transmission increases with the natural convective heat transfer dominating the conductive energy transport. The motion intensity reduces with increasing the vortex viscosity, weakening its ability in convective energy transport and reducing Nu.

Fig. 11 demonstrates the mean Nusselt number variation by Hartmann number and radiation parameter at two different Rayleigh numbers. According to this figure, although an increase in the Hartmann number, meaning a greater Lorentz force effect on the fluid particles, does not change the mean Nu at low Ra ($Ra = 10$), Ha and the Lorentz force can affect the Nusselt number through increasing the buoyancy at high Rayleigh numbers ($Ra = 10^3$). Under these conditions, Nu_{avg} reduces with an increment of Ha. This effect has a limited amplitude, which continues to approximately $Ha = 10$, after which the mean Nusselt number becomes independent on the Hartmann number again, due to the weakening of the buoyancy force.

5. Conclusion

MHD natural convection and thermal radiation of micropolar nanoliquid in a square porous chamber with centered isothermal elliptical heat source have been studied. A complex analysis for liquid circulation and energy transport combined with average Nusselt number has been computationally conducted by the finite element method. The

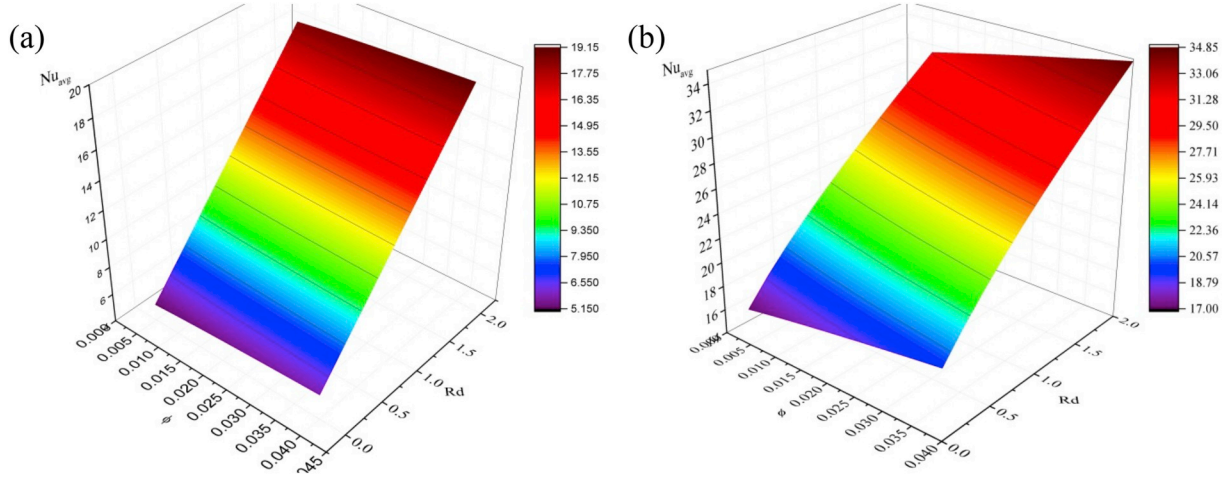

Fig. 8. Surface variation of Nu_{avg} (a) $Ra = 10$ and (b) $Ra = 10^3$ with radiation parameter and volume fraction of nanoparticles.

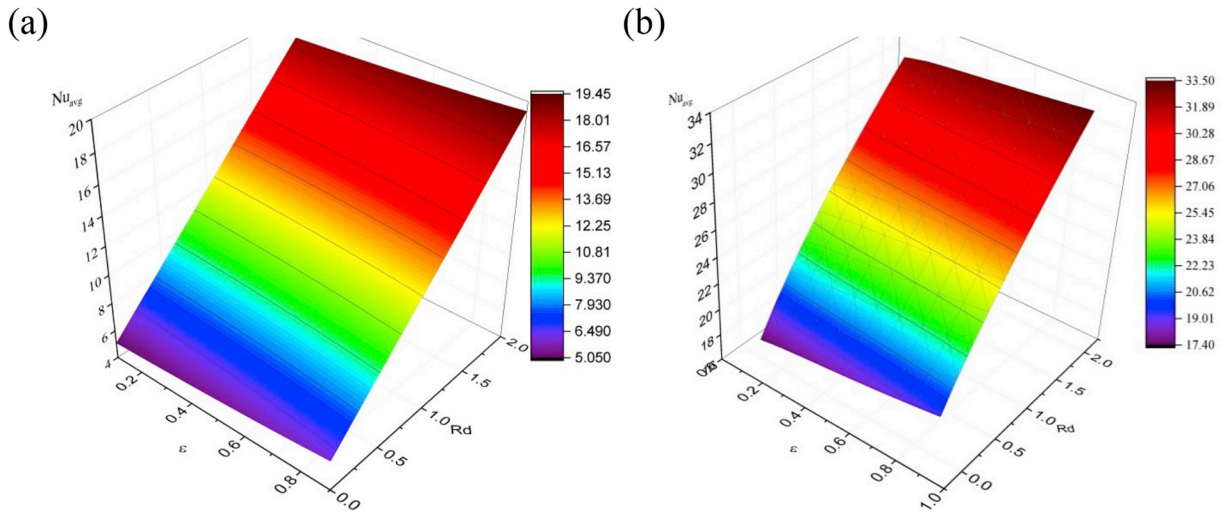

Fig. 9. Surface variation of Nu_{avg} (a) $Ra = 10$ and (b) $Ra = 10^3$ with radiation parameter and porosity coefficient.

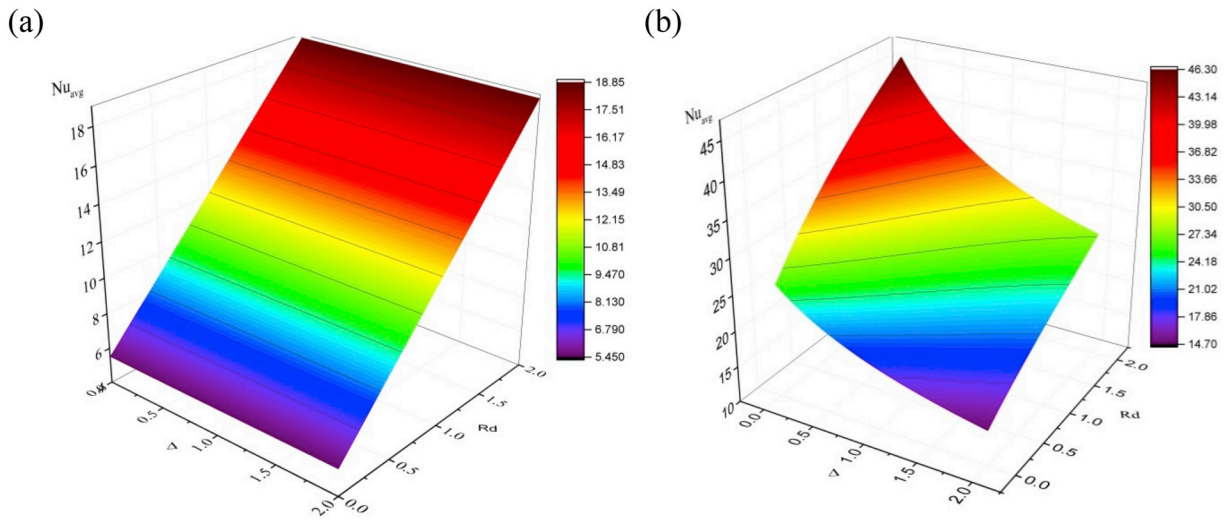

Fig. 10. Surface variation of Nu_{avg} (a) $Ra = 10$ and (b) $Ra = 10^3$ with radiation parameter and vortex viscosity.

governing characteristics for the present study were the Darcy–Rayleigh number $Ra = 10$–1000, porosity $\varepsilon = 0.1$–0.9, Darcy number $Da = 10^{-5}$–10^{-1}, radiation parameter $R_d = 0$–2, Hartmann number $Ha = 0$–50, nanoparticles concentration $\phi = 0$–0.04, and vortex viscosity characteristic $\Delta = 0$–2. The streamlines, isotherms and isolines of microrotation combined with the mean Nusselt number for mentioned governing characteristics have been studied. The following results have been revealed:

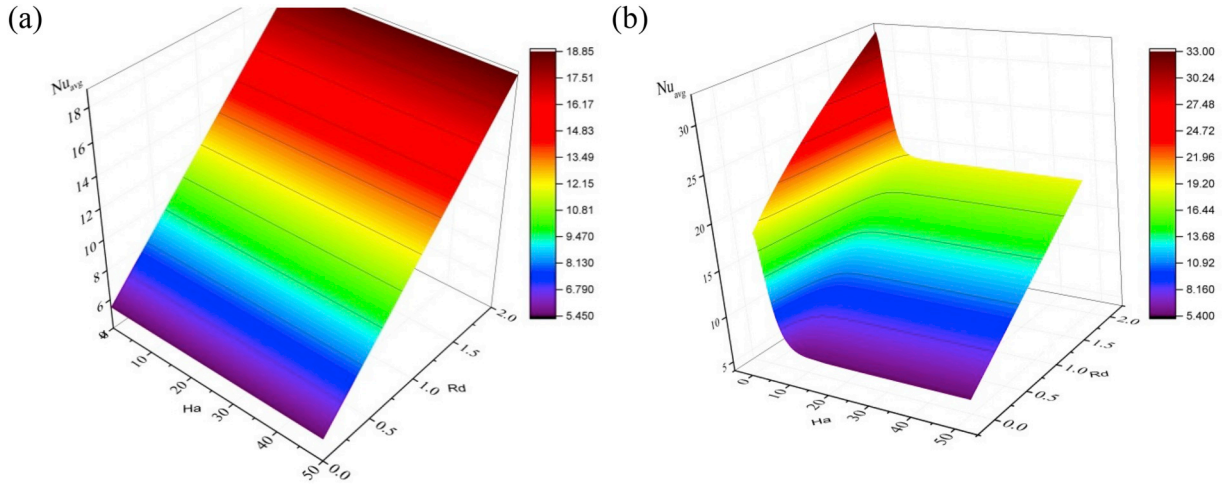

Fig. 11. Surface variation of Nu_{avg} (a) $Ra = 10$ and (b) $Ra = 10^3$ with Hartmann number and radiation parameter.

- A rise of Ra leads to the thermal transmission intensification and nanofluid circulation strengthening.
- High Ra numbers illustrate a drift of convective cells cores in the upper part over the heated element.
- A rise of the thermal radiation parameter illustrates a growth of both Nu_{avg} and nanofluid circulation intensity.
- The effect of porosity is more visible for high Ra and low values of the thermal radiation parameter, namely, a growth of ε results in the convective energy transport intensification.
- Increment of ϕ and R_d increases Nu_{avg}, that is more significant for high Ra.
- Average Nusselt number reduces with an increment of Ha for high Ra, while for low Ra a weak change of Nu_{avg} can be found.
- Behavior of microrotation can be described using the streamlines.
- A growth of the vortex viscosity characteristic reflects the thermal transmission suppression and convective motion attenuation inside the cavity.

Acknowledgments

This work of I. Pop has been supported from the grant PN-III-P4-ID-PCE-2016-0036, UEFISCDI, Romania. This work of M. Sheremet has been supported by the Russian Science Foundation (Project No. 17-79-20141).

References

[1] Z. Shah, S. Islam, H. Ayaz, S. Khan, Radiative heat and mass transfer analysis of micropolar nanofluid flow of Casson fluid between two rotating parallel plates with effects of hall current, J. Heat Transf. 141 (2019) 022401.
[2] Z. Shah, S. Islam, T. Gul, E. Bonyah, M. Altaf Khan, The electrical MHD and hall current impact on micropolar nanofluid flow between rotating parallel plates, Results Phys. 9 (2018) 1201–1214.
[3] A.C. Eringen, Simple microfluids, Int. J. Eng. Sci. 2 (1964) 205–217.
[4] A.C. Eringen, Theory of micropolar fluids, J. Math. Mech. (1966) 1–18.
[5] A.C. Eringen, Microcontinuum field theories: I, Foundations and Solids, Springer Science & Business Media, 2012.
[6] T. Javed, M.A. Siddiqui, Energy transfer through mixed convection within square enclosure containing micropolar fluid with non-uniformly heated bottom wall under the MHD impact, J. Mol. Liq. 249 (2018) 831–842.
[7] A. Ahmed, S. Nadeem, Effects of magnetohydrodynamics and hybrid nanoparticles on a micropolar fluid with 6-types of stenosis, Results Phys. 7 (2017) 4130–4139.
[8] M.A. Sheremet, I. Pop, A. Ishak, Time-dependent natural convection of micropolar fluid in a wavy triangular cavity, Int. J. Heat Mass Transf. 105 (2017) 610–622.
[9] M. Muthtamilselvan, K. Periyadurai, D.H. Doh, Effect of uniform and nonuniform heat source on natural convection flow of micropolar fluid, Int. J. Heat Mass Transf. 115 (2017) 19–34.
[10] M. Muthtamilselvan, K. Periyadurai, D.H. Doh, Impact of nonuniform heated plate on double-diffusive natural convection of micropolar fluid in a square cavity with Soret and Dufour effects, Adv. Powder Technol. 29 (2018) 66–77.
[11] S. Siddiqa, A. Faryad, N. Begum, M.A. Hossain, R.S.R. Gorla, Periodic magnetohydrodynamic natural convection flow of a micropolar fluid with radiation, Int. J. Therm. Sci. 111 (2017) 215–222.
[12] S.U.S. Choi, J.A. Eastman, Enhancing thermal conductivity of fluids with nanoparticles, Argonne National Lab, IL (United States), 1 January 1995.
[13] H. Masuda, A. Ebata, K. Teramae, Alteration of thermal conductivity and viscosity of liquid by dispersing ultra-fine particles, Dispersion of Al2O3, SiO2 and TiO2 ultra-fine particles, 1993.
[14] S. Mehryan, M. Izadi, A.J. Chamkha, M.A. Sheremet, Natural convection and entropy generation of a ferrofluid in a square enclosure under the effect of a horizontal periodic magnetic field, J. Mol. Liq. 263 (2018) 510–525.
[15] R. Mohebbi, M. Izadi, A. Amiri Delouei, H. Sajjadi, Effect of MWCNT-Fe_3O_4/water hybrid nanofluid on the thermal performance of ribbed channel with apart sections of heating and cooling, J. Therm. Anal. Calorim. 135 (2019) 3029–3042.
[16] M. Izadi, R. Mohebbi, A. Chamkha, I. Pop, Effects of cavity and heat source aspect ratios on natural convection of a nanofluid in a C-shaped cavity using Lattice Boltzmann method, Int. J. Num. Methods Heat Fluid Flow 28 (2018) 1930–1955.
[17] M. Izadi, A. Behzadmehr, M.M. Shahmardan, Effects of inclination angle on mixed convection heat transfer of a nanofluid in a square cavity, Int. J. Comput. Methods Eng. Sci. Mech. 16 (2015) 11–21.
[18] R. Mohebbi, M. Izadi, A.J. Chamkha, Heat source location and natural convection in a C-shaped enclosure saturated by a nanofluid, Phys. Fluids 29 (2017) 122009.
[19] M. Izadi, R. Mohebbi, D. Karimi, M.A. Sheremet, Numerical simulation of natural convection heat transfer inside a$^{\perp}$ shaped cavity filled by a MWCNT-Fe_3O_4/water hybrid nanofluids using LBM, Chem. Eng. Process. Process Intensif. 125 (2018) 56–66.
[20] G. Hoghoughi, M. Izadi, H.F. Oztop, N. Abu-Hamdeh, Effect of geometrical parameters on natural convection in a porous undulant-wall enclosure saturated by a nanofluid using Buongiorno's model, J. Mol. Liq. 255 (2018) 148–159.
[21] R. Mohebbi, M.M. Rashidi, M. Izadi, N.A.C. Sidik, H.W. Xian, Forced convection of nanofluids in an extended surfaces channel using lattice Boltzmann method, Int. J. Heat Mass Transf. 117 (2018) 1291–1303.
[22] M. Izadi, M.M. Shahmardan, M. Norouzi, A. Rashidi, A. Behzadmehr, Cooling performance of a nanofluid flow in a heat sink microchannel with axial conduction effect, Appl. Phys. A Mater. Sci. Process. 117 (2014) 1821–1833.
[23] M. Izadi, M.M. Shahmardan, M.J. Maghrebi, A. Behzadmehr, Numerical study of developed laminar mixed convection of Al_2O_3/water nanofluid in an annulus, Chem. Eng. Commun. 200 (2013) 878–894.
[24] M. Izadi, A. Behzadmehr, M.M. Shahmardan, Effects of discrete source-sink arrangements on mixed convection in a square cavity filled by nanofluid, Korean J. Chem. Eng. 31 (2014) 12–19.
[25] A.J. Chamkha, M.A. Ismael, Conjugate heat transfer in a porous cavity filled with nanofluids and heated by a triangular thick wall, International Journal of Thermal Sciences 67 (2013) 135–151.
[26] A. Chamkha, M. Ismael, A. Kasaeipoor, T. Armaghani, Entropy generation and natural convection of CuO-water nanofluid in C-shaped cavity under magnetic field, Entropy 18 (2016) 50.
[27] N. Ben-Cheikh, A.J. Chamkha, B. Ben-Beya, T. Lili, Natural convection of water-based nanofluids in a square enclosure with non-uniform heating of the bottom wall, J. Mod. Phys. 4 (2013) 147–159.
[28] A.I. Alsabery, R. Mohebbi, A.J. Chamkha, I. Hashim, Effect of local thermal non-equilibrium model on natural convection in a nanofluid-filled wavy-walled porous cavity containing inner solid cylinder, Chem. Eng. Sci. 201 (2019) 247–263.
[29] A.I. Alsabery, T. Armaghani, A.J. Chamkha, M.A. Sadiq, I. Hashim, Effects of two-phase nanofluid model on convection in a double lid-driven cavity in the presence of a magnetic field, Int. J. Num. Methods Heat Fluid Flow 29 (2019) 1272–1299.
[30] A.I. Alsabery, M.A. Sheremet, A.J. Chamkha, I. Hashim, Impact of nonhomogeneous nanofluid model on transient mixed convection in a double lid-driven wavy cavity involving solid circular cylinder, Int. J. Mech. Sci. 150 (2019) 637–655.
[31] M.A. Ismael, T. Armaghani, A.J. Chamkha, Conjugate heat transfer and entropy generation in a cavity filled with a nanofluid-saturated porous media and heated by

a triangular solid, J. Taiwan Inst. Chem. Eng. 59 (2016) 138–151.
[32] S. Nasir, Z. Shah, S. Islam, E. Bonyah, T. Gul, Darcy Forchheimer nanofluid thin film flow of SWCNTs and heat transfer analysis over an unsteady stretching sheet, AIP Adv. 9 (2019) 15223.
[33] R. Nasrin, M.A. Alim, A.J. Chamkha, Combined convection flow in triangular wavy chamber filled with water–CuO nanofluid: effect of viscosity models, Int. Commun. Heat Mass Transf. 39 (2012) 1226–1236.
[34] R. Nasrin, M.A. Alim, A.J. Chamkha, Modeling of mixed convective heat transfer utilizing nanofluid in a double lid-driven chamber with internal heat generation, Int. J. Num. Methods Heat Fluid Flow 24 (2014) 36–57.
[35] S. Parvin, A.J. Chamkha, An analysis on free convection flow, heat transfer and entropy generation in an odd-shaped cavity filled with nanofluid, Int. Commun. Heat Mass Transf. 54 (2014) 8–17.
[36] F. Selimefendigil, H.F. Öztop, A.J. Chamkha, MHD mixed convection and entropy generation of nanofluid filled lid driven cavity under the influence of inclined magnetic fields imposed to its upper and lower diagonal triangular domains, J. Magn. Magn. Mater. 406 (2016) 266–281.
[37] Z. Shah, A. Dawar, E.O. Alzahrani, P. Kumam, A.J. Khan, S. Islam, Hall effect on couple stress 3D nanofluid flow over an exponentially stretched surface with Cattaneo–Christov heat flux model, IEEE Access 7 (2019) 64844–64855.
[38] M. Sheikholeslami, M. Shamlooei, Fe_3O_4–H_2O nanofluid natural convection in presence of thermal radiation, Int. J. Hydrog. Energy 42 (2017) 5708–5718.
[39] S. Nasir, Z. Shah, S. Islam, W. Khan, S.N. Khan, Radiative flow of magneto hydrodynamics single-walled carbon nanotube over a convectively heated stretchable rotating disk with velocity slip effect, Adv. Mech. Eng. 11 (2019) 1–11.
[40] Z. Shah, A. Dawar, P. Kumam, W. Khan, S. Islam, Impact of nonlinear thermal radiation on MHD nanofluid thin film flow over a horizontally rotating disk, Appl. Sci. 9 (2019) 1533.
[41] Z. Shah, E. Bonyah, S. Islam, T. Gul, Impact of thermal radiation on electrical MHD rotating flow of carbon nanotubes over a stretching sheet, AIP Adv. 9 (2019) 15115.
[42] M. Ghalambaz, A. Doostani, E. Izadpanahi, A.J. Chamkha, Phase-change heat transfer in a cavity heated from below: the effect of utilizing single or hybrid nanoparticles as additives, J. Taiwan Inst. Chem. Eng. 72 (2017) 104–115.
[43] M. Mansour, M. Bakeir, A. Chamkha, Natural convection inside a C-shaped nanofluid-filled enclosure with localized heat sources, Int. J. Num. Methods Heat Fluid Flow 24 (2014) 1954–1978.
[44] M. Sheikholeslami, Z. Shah, A. Shafee, I. Khan, I. Tlili, Uniform magnetic force impact on water based nanofluid thermal behavior in a porous enclosure with ellipse shaped obstacle, Sci. Rep. 9 (2019) 1196.
[45] M. Sheikholeslami, Z. Shah, A. Tassaddiq, A. Shafee, I. Khan, Application of electric field for augmentation of ferrofluid heat transfer in an enclosure including double moving walls, IEEE Access 7 (2019) 21048–21056.
[46] Z. Li, M. Sheikholeslami, Z. Shah, A. Shafee, A.-R. Al-Qawasmi, I. Tlili, Transient process in a finned triplex tube during phase changing of aluminum oxide enhanced PCM, Eur. Phys. J. Plus 134 (2019) 173.
[47] S.A. Mehryan, M. Izadi, M.A. Sheremet, Analysis of conjugate natural convection within a porous square enclosure occupied with micropolar nanofluid using local thermal non-equilibrium model, J. Mol. Liq. 250 (2018) 353–368.
[48] G.C. Bourantas, V.C. Loukopoulos, Modeling the natural convective flow of micropolar nanofluids, Int. J. Heat Mass Transf. 68 (2014) 35–41.
[49] A. Hussanan, M.Z. Salleh, I. Khan, S. Shafie, Convection heat transfer in micropolar nanofluids with oxide nanoparticles in water, kerosene and engine oil, J. Mol. Liq. 229 (2017) 482–488.
[50] J. Buongiorno, Convective transport in nanofluids, J. Heat Transf. 128 (2006) 240–250.
[51] T. Hayat, M.I. Khan, M. Waqas, A. Alsaedi, M.I. Khan, Radiative flow of micropolar nanofluid accounting thermophoresis and Brownian moment, Int. J. Hydrog. Energy 42 (2017) 16821–16833.
[52] M. Izadi, R. Mohebbi, A.A. Delouei, H. Sajjadi, Natural convection of a magnetizable hybrid nanofluid inside a porous enclosure subjected to two variable magnetic fields, Int. J. Mech. Sci. 151 (2019) 154–169.
[53] S. Mehryan, M.A. Sheremet, M. Soltani, M. Izadi, Natural convection of magnetic hybrid nanofluid inside a double-porous medium using two-equation energy model, J. Mol. Liq. 277 (2019) 959–970.
[54] M. Izadi, S. Sinaei, S. Mehryan, H.F. Oztop, N. Abu-Hamdeh, Natural convection of a nanofluid between two eccentric cylinders saturated by porous material: Buongiorno's two phase model, Int. J. Heat Mass Transf. 127 (2018) 67–75.
[55] S. Mehryan, M. Ghalambaz, M. Izadi, Conjugate natural convection of nanofluids inside an enclosure filled by three layers of solid, porous medium and free nanofluid using Buongiorno's and local thermal non-equilibrium models, J. Therm. Anal. Calorim. 135 (2019) 1047–1067.
[56] Z. Shah, A. Dawar, S. Islam, I. Khan, D.L.C. Ching, Darcy-Forchheimer flow of radiative carbon nanotubes with microstructure and inertial characteristics in the rotating frame, Case Stud. Thermal Eng. 12 (2018) 823–832.
[57] A.I. Alsabery, H. Saleh, I. Hashim, Effects of viscous dissipation and radiation on MHD natural convection in oblique porous cavity with constant heat flux, Adv. Appl. Math. Mech. 9 (2017) 463–484.
[58] M. Sheikholeslami, Solidification of NEPCM under the effect of magnetic field in a porous thermal energy storage enclosure using CuO nanoparticles, J. Mol. Liq. 263 (2018) 303–315.
[59] A.J. Chamkha, A.-R.A. Khaled, Hydromagnetic combined heat and mass transfer by natural convection from a permeable surface embedded in a fluid-saturated porous medium, Int. J. Num. Methods Heat Fluid Flow 10 (2000) 455–477.
[60] A.J. Chamkha, H. Al-Naser, Double-diffusive convection in an inclined porous enclosure with opposing temperature and concentration gradients, Int. J. Therm. Sci. 40 (2001) 227–244.
[61] A.J. Chamkha, Double-diffusive convection in a porous enclosure with cooperating temperature and concentration gradients and heat generation or absorption effects, Num. Heat Transf. A 41 (2002) 65–87.
[62] A. Chamkha, Solar radiation assisted natural convection in uniform porous medium supported by a vertical flat plate, J. Heat Transf. 119 (1997) 89–96.
[63] H. Hashemi, Z. Namazian, S.A. Mehryan, Cu-water micropolar nanofluid natural convection within a porous enclosure with heat generation, J. Mol. Liq. 236 (2017) 48–60.
[64] S.E. Ahmed, M.A. Mansour, A.K. Hussein, S. Sivasankaran, Mixed convection from a discrete heat source in enclosures with two adjacent moving walls and filled with micropolar nanofluids, Eng. Sci. Technol. Int. J. 19 (2016) 364–376.
[65] C. Sivaraj, M.A. Sheremet, Natural convection coupled with thermal radiation in a square porous cavity having a heated plate inside, Transp. Porous Media 114 (2016) 843–857.
[66] M. Izadi, S.A. Mehryan, M.A. Sheremet, Natural convection of CuO-water micropolar nanofluids inside a porous enclosure using local thermal non-equilibrium condition, J. Taiwan Inst. Chem. Eng. 88 (2018) 89–103.
[67] M. Izadi, S.A. Mohammadi, S.A.M. Mehryan, T. Yang, M.A. Sheremet, Thermogravitational convection of magnetic micropolar nanofluid with coupling between energy and angular momentum equations, International Journal of Heat and Mass Transfer 145 (2019) 118748.
[68] A.J. Chamkha, M.A. Ismael, Natural convection in differentially heated partially porous layered cavities filled with a nanofluid, Num. Heat Transf. A 65 (2014) 1089–1113.
[69] J.P. Garandet, T. Alboussiere, R. Moreau, Buoyancy driven convection in a rectangular enclosure with a transverse magnetic field, Int. J. Heat Mass Transf. 35 (1992) 741–748.
[70] J. Koo, C. Kleinstreuer, Laminar nanofluid flow in microheat-sinks, Int. J. Heat Mass Transf. 48 (2005) 2652–2661.
[71] J. Li, Computational analysis of nanofluid flow in microchannels with applications to micro-heat sinks and bio-MEMS, Ph.D. Thesis, USA, 2008.
[72] H.F. Oztop, E. Abu-Nada, Numerical study of natural convection in partially heated rectangular enclosures filled with nanofluids, Int. J. Heat Fluid Flow 29 (2008) 1326–1336.
[73] H. Hashemi, Z. Namazian, S.M.H. Zadeh, S.A. Mehryan, MHD natural convection of a micropolar nanofluid flowing inside a radiative porous medium under LTNE condition with an elliptical heat source, J. Mol. Liq. 271 (2018) 914–925.
[74] J. Donea, A. Huerta, Finite Element Methods for Flow Problems, John Wiley & Sons, 2003.
[75] P. Wriggers, Nonlinear Finite Element Methods, Springer Science & Business Media (2008).
[76] Q. Sun, I. Pop, Free convection in a triangle cavity filled with a porous medium saturated with nanofluids with flush mounted heater on the wall, Int. J. Therm. Sci. 50 (2011) 2141–2153.
[77] O. Aydın, I. Pop, Natural convection in a differentially heated enclosure filled with a micropolar fluid, Int. J. Therm. Sci. 46 (2007) 963–969.